Observations of microscale tensile fatigue damage mechanisms of composite materials for wind turbine blades

Mikkelsen, Lars Pilgaard

Published in:
I O P Conference Series: Materials Science and Engineering

Link to article, DOI:
10.1088/1757-899X/388/1/012006

Publication date:
2018

Document Version
Publisher's PDF, also known as Version of record

Observations of microscale tensile fatigue damage mechanisms of composite materials for wind turbine blades

IOP Conf. Series: Materials Science and Engineering **388** (2018) 012006 doi:10.1088/1757-899X/388/1/012006

Observations of microscale tensile fatigue damage mechanisms of composite materials for wind turbine blades

L P Mikkelsen

Section of Composite Mechanics and Structures, DTU Wind Energy, Technical University of Denmark, 4000 Roskilde, Denmark

E-mail: lapm@dtu.dk

Abstract. In the presented study, it has been studied how tensile/tensile fatigue damage will develop in quasi-unidirectional non-crimp fabric based glass fibre epoxy matrix composites. A material system conventionally used as the load carrying laminates in wind turbine blades. It will be demonstrated by stopping a tensile/tensile fatigue test before the final material failure, how 3D X-ray computer tomography (x-ray CT) can be used for determining fibre failure inside the composite material. Due to the rather coarse bundle-structure of the non-crimp fabrics investigated, a relative large cross section area of the test-sample is necessary in order for testing a representative material volume. Therefore, the x-ray CT technique is used in a scout and zoom test-setup where a scout scan of the 15 mm large cross-section is used for identifying the damage region, while the subsequently zoom scan of a 2-3 mm field of view region is used for determine the fibre failures. This scan-setup is non-destructive, and it is therefore possible to obtain a number of scans during the fatigue damage development. Thereby, it is found that the fibre failure are mainly occurring close to points where the load carrying uni-directional fibre bundles are in close contact with the crossing points of secondary oriented fibre bundles, the so-called backing bundles.

1. Introduction

The load carrying laminates in modern large wind turbine blades are often based on non-crimp fabric reinforced composites. Contrary to a woven fabric, a non-crimp fabric is buildup of straight bundles stitched to a thin backing layer. Thereby, waviness of the stiffness giving fibers are avoided and larger material stiffness are achieved. In a typical quasi-unidirectional non-crimp fabric used in the wind turbine industry, around 90% of the fibers are oriented in the load direction. The remaining 10% is secondary oriented bundles with a much lower tex-values (thinner bundles). The fact that not all fibers are oriented in one direction is the reason for the term “quasi-unidirectional”, which we will use in the following. The load carrying laminates in a wind turbine is due to the requirement of large stiffness and fatigue resistance [1] to a large degree buildup of such quasi-unidirectional non-crimp fabrics resulting in wind turbine blades where more than 60% of the fibers are in the axial direction of the blade [2].

Through the last couple of years, comprehensive studies of the fatigue damage mechanism in quasi-unidirectional non-crimp fabrics based composites has been performed non-destructive using 3D x-ray computer tomography [3]–[5]. Studies which has been enhanced the fatigue damage mechanisms obtained in earlier destructive fatigue damage characterizations of similar non-crimp fabric based glass fiber composites [6]. From the studies it has been observed that transverse tunnel cracks in the backing bundles will develops in the initial phase of the fatigue loading. Those cracks will subsequently grow into the load carrying fiber bundles as local fiber breakages. Finally, those fiber breakages will localize

into the final failure of the test sample. Each of those three damage mechanisms can also be identified on the measured stiffness degradation where first a small rapid stiffness drop will occur at the initiation phase, a stable stiffness degradation region fiber breakage phase and a fast large stiffness drop for the localization phase. A stiffness degradation curve rather similar to the three main stages for fatigue damage of fiber composites reported by Reifsnider and Jamison [7] for pre-preg composites. Nevertheless, the failure mechanism in the non-crimp fabric differ from that observed for the pre-preg based composites due to the difference in the fiber architecture.

In the present study, a non-crimp fabric based high-module (E_f = 80GPa) glass-fiber epoxy matrix material system used in the wind turbine blade industry is investigated. It is demonstrated how thermovision can be used for identification of the initial damage region in a tensile/tensile fatigue test coupon. In addition, the observed material stiffness degradation can be used for identify how far we are into the fatigue damage region. The fatigue damage is characterized using a scout and zoom 3D x-ray scan sequence. Thereby, it is possible to identify a small damage region inside a field of view of 2-3 mm. Only by using such small a field of view, it is possible to identify the single fiber failure of the 17 µm thick glass fibers.

2. Material system

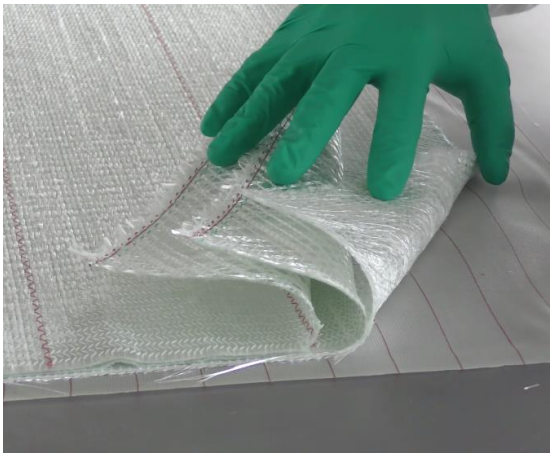

(a) Three of the 6 non-crimp fabrics used in the symmetric layup

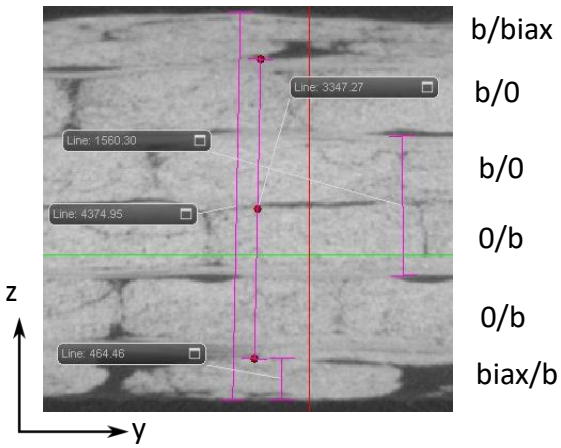

(b) A 2D slice from the X-ray scan of the full cross section of the composite

Figure 1. The $[b/biax,b/0,b/0]_s$ glass fibre non-crimp fabric layup with the backing pointing outward from the centre is used in the study

A 6 layer glass fiber composite is studied where the layup is $[b/biax,b/0,b/0]_s$ as seen in Figure 1a. Only the fatigue damage located inside the quasi-unidirectional non-crimp layers in the center of the sample is investigated.

The 4 quasi-unidirectional fabrics denoted 'b/0' is made by 1152g/m^2 unidirectional bundles each with a tex value (weight per km bundle) on 2400 g/km with an average fiber diameter on D_0=17 µm. With a glass fiber density on $\rho_{glass} = 2.6g/cm^3$ this will correspond to approximately 4000 fibers in each UD bundles. The UD bundles are stitched using a polyester yarn to a backing layer consist of ±45 and 90 oriented bundles with a tex value of 200 g/km and an average fiber diameter on D_b=16 µm. The backing bundles are does therefore consist of approximately 380 fibers. The area weight of the ±45° bundles is 100g/m^2 and the 90° bundles is 19g/m^2.

The two biax fabrics denoted 'b/biax' is made of 2x296g/m^2 ±45° oriented fiber bundles each with a tex value on 600g/km with an average fiber diameter on $D_{\pm}$45=16 µm corresponding to 1150 fibers in each bundles. In addition, the biax fabrics does also have 19 g/m^2 90° bundles each with a tex value on

200 g/km. Those bundles are stitched to a Chopped strand Mat (CSM) with an area weight on 100 g/m^2. Except from the CSM mat, where the fibers is standard E-glass with a stiffness on $E_f = 72GPa$ all the other fibers are high-modulus fibers with on $E_f = 80GPa$.

After stacking the non-crimp fabrics, the composite is manufactured using vacuum assisted transfer molding using a Huntsman epoxy denoted: Aralide LY 1564SP/XB3486. The laminates was cured using a two-stage cure profile first with a pre-cure at 50C for 7 hours followed by a post-cure sequence on 90C in 3 hours. The thickness of the resulting composite was approximately 2.3mm which corresponds to a fiber volume fraction on 57%.

3. Tension/tension fatigue testing

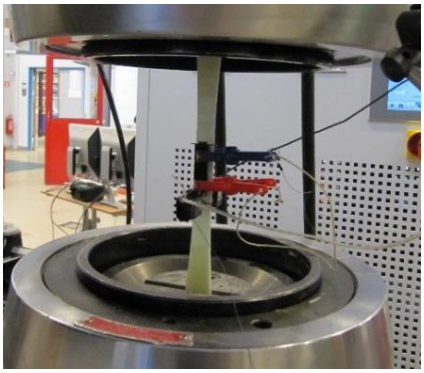

(a) Test-setup with back-to-back mounted extensometers for stiffness degradation measurement

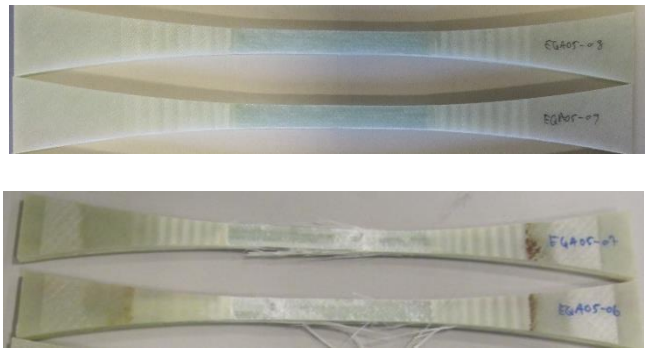

(b) Test sample before and after the test

Figure 2. Tension/tension fatigue testing

The test coupon is fatigue loaded cyclic in tension/tension under prescribed loads with a fixed R-ratio given by $R = \frac{\sigma_{min}}{\sigma_{max}} = 0.1$. Figure 2a show the experimental setup for the samples tested to final failure. In here, two extensometers are mounted back-to-back in order to measure the stiffness degradation of the material. A butterfly shaped specimen [8] is used in the test, as it can be seen in figure 2b. In order to have a representative volume of material in the central part of the test coupons, a constant cross-section on 15×4.5mm^2 over a gauge length of 60mm is used. The total length of the test-sample is 410mm with a maximum sample width in the gripping region of 50mm.

Figure 3a show the SN-curve obtained during the fatigue test of 8 test-samples at different load levels. The load level of the test material is inhere presented as a normalization of the prescribed maximum stress σ_{max} with respect to the initial stiffness E_0 of the test-sample. The normalization maximum stress is denoted by $\varepsilon_{max} = \sigma_{max}/E_0$. A Basquin curve $N_{fail} = K\varepsilon_{max}^m$ is fitted to the measured fatigue failure SN-points. Together with the fatigue test tested until final failure, figure 3 also include the data for a test sample stopped 10.000 cycles before the expected material failure (marked with the red point on the SN-curve). The material damage inside this sample is subsequently studied using 3D x-ray CT scan presented in the next section. Figure 3b show the corresponding stiffness degradation of the test-material. The composite material stiffness degradation is measured over the full load cycle using the back-to-back mounted 50mm/±2 mm extensometers inside the gauge section. The three main stages for fatigue damage evolution as reported by e.g. Reifsnider and Jamison [7] with (stage I) an initial fast stiffness drop during the initial cyclic loadings, (stage II) a rather constant stiffness degradation over the major second stage fatigue life and (stage III) a fast stiffness degradation in the third stage just before

the final fatigue damage localization in the material. The fatigue damage evolution has been investigated in details in [5] and [4] where [5] mainly investigated the initial fatigue damage govern by the transverse cracking of the backing bundles related mainly to the initial stage I of the stiffness degradation, while [4] investigate the progression of the fiber breakages in the load carrying fibers related to stage II. The red stiffness degradation curve shown in figure 3b is the stiffness degradation of the x-ray studied sample where the end-point of the red curve correspond to the red point in figure 3a. It should be noted that the stiffness degradation curve for the x-ray studied sample has been obtained without extensometers so it was possible to measure the surface temperature of the test sample as shown in figure 4. The red stiffness degradation curve is obtained from the overall test sample stiffness degradation which also can include effect of tab delamination and damage in the gripping region. Nevertheless, the curve is found to follow the other curves quite well.

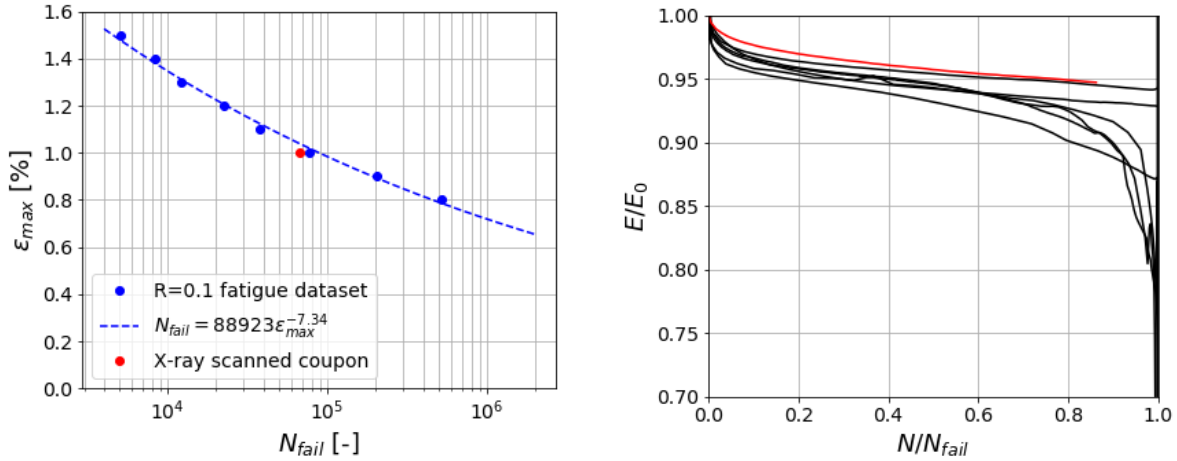

(a) SN-curve for the normalized stress versus number of cycles to failure

(b) Stiffness degradation caused by the fatigue damage development

Figure 3. Results from the R=0.1 load controlled tension/tension fatigue testing

In figure 4, the surface temperature of the test-sample and the corresponding stiffness degradation curve is shown for a test specimen denoted EQA05-14 which is the test-sample stopped after 67000 load cycles and therefore 10.000 cycles before the expected lifetime of the specimen. In the figure there is a QR-code which are linking to a video showing the development of this temperature profile. A URL of the same link can also be found in the figure caption. From the temperature profile, it can be seen that there are some self-heating going on near the end of the tabs which are properly related to tab-delamination similar to what has been found by [9]. In addition, close to the stopping point (see the video), there was observed a hot spot in the center of the test-sample. It is this point which in the next section will turn out to be an active fatigue damage region with a lot of fiber breakages.

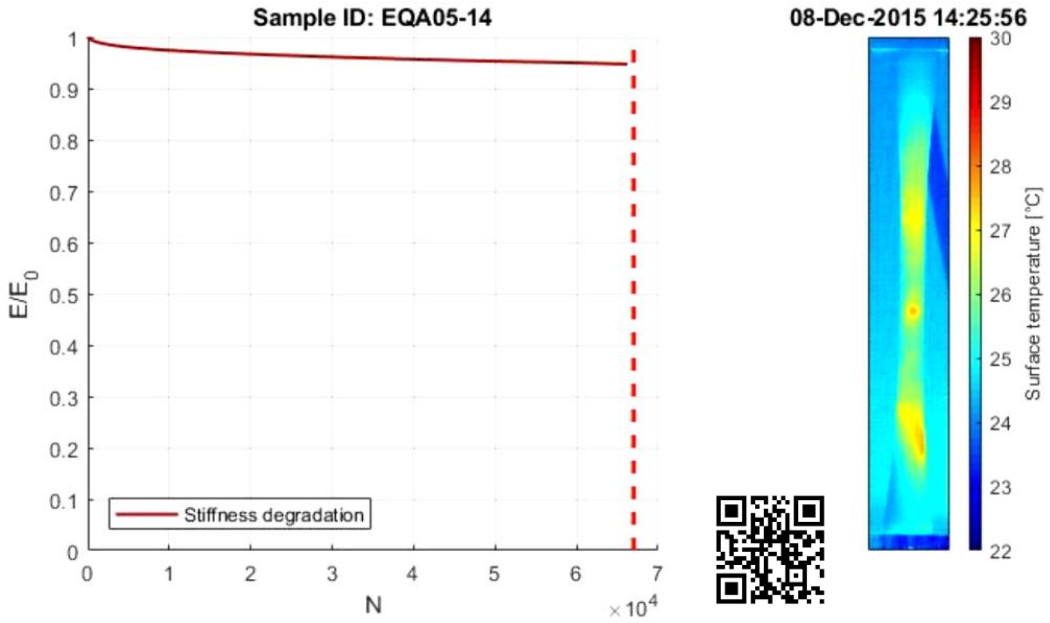

Figure 4. Test-sample stiffness degradation and surface temperature of the x-ray scanned specimen. A link to the video use the QR-code on a mobile phone or use the link (https://youtu.be/UkPjghocsTg).

4. Scout and zoom scan

After 67000 cycles, the central part of the test-sample, see figure 5a was investigated using a so-called scout and zoom scan sequence using a Zeiss Xradia Versa 520 x-ray scanning machine. The scout scan, figure 5b, is used for identifying the region of interest, a region which subsequently is scanned at a much higher resolution, figure 5c. Table 1 show the scan-setting for the two scans. The data and tiff-stack from the two scans can be downloaded from [10].

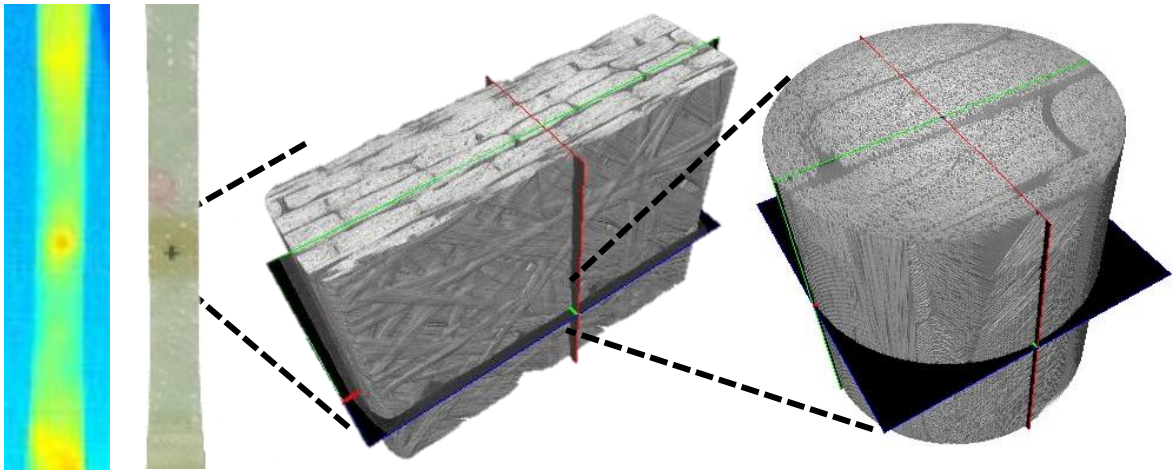

(a) Central part of test sample

(b) Large field of view: 15x15x4.5mm^3

(c) Small field of view: 2.5x2.5x2.5 mm^3

Figure 5. Scout and zoom scan

Table 1. Scan-setting

	Source to sample [mm]	Detector to sample [mm]	Exposer time [s]	No. of project. [-]	Accel. voltage [keV]	Bin-ning	Pixel size [µm]	Optical magnifi-cation	Scan time [hours]
Scout (LFoV)	28	91	2	801	50	2	16.1114	0.4	0.5
Zoom (SFoV)	28	47	15	3201	70	2	2.5043	4	13.3

Figure 6, present selected slices from the scout scan. Despite the large voxel size on 16 µm, it is possible to see indication on damage in a region of the scan. A region which on the slice in figure 6 is marked by a white box. A reconstructed 3D x-ray scan is a 3-D image which in figure 6 is shown as a set of selected 2D slices. Trying identifying damage region in composite materials it is often must better slicing through the 3D reconstructed image instead of looking on single 2D slices. Therefore, all the images in figure 6 includes a link with a QR-code and a URL-link to videos of slicing through the 3D reconstructed image. From the videos, the damage region show up rather clear and from that, the coordinates for the zoomed scan can be defined. The zoomed scan shown in figure 7 is a scan of the region defined by the white box shown in figure 6.

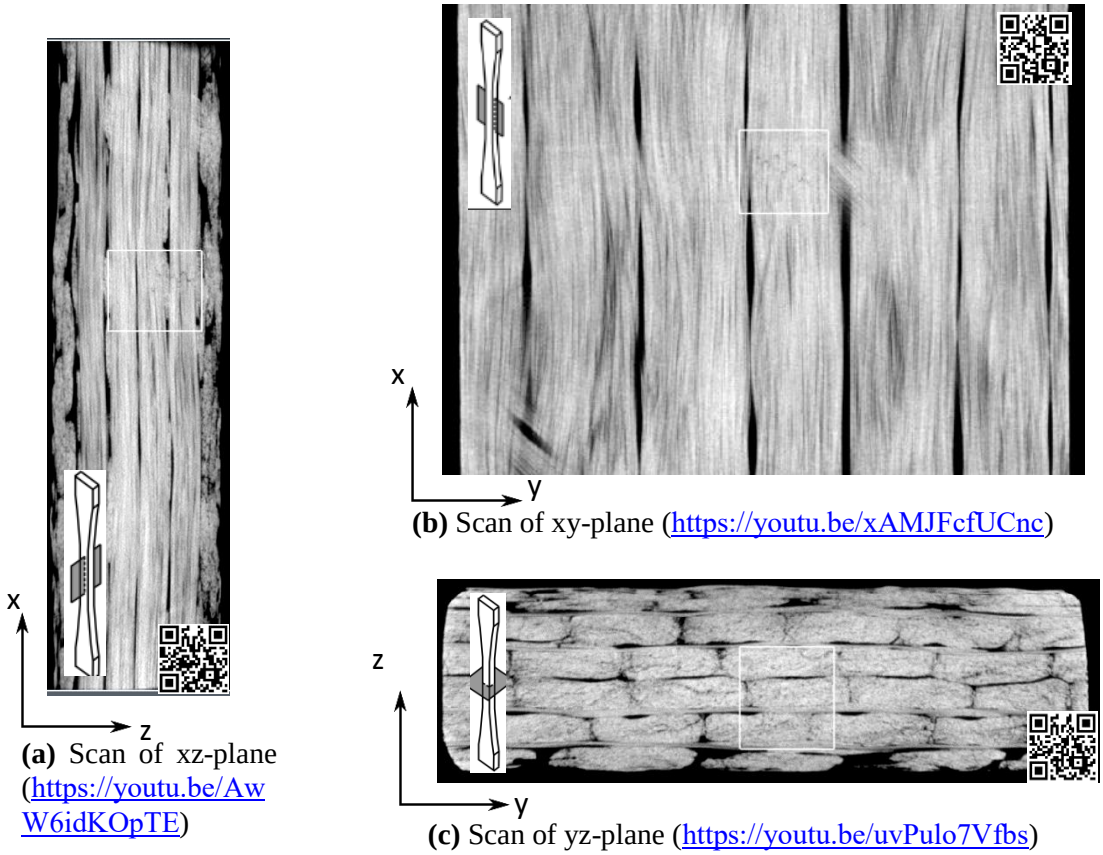

(a) Scan of xz-plane (https://youtu.be/AwW6idKOpTE)

(b) Scan of xy-plane (https://youtu.be/xAMJFcfUCnc)

(c) Scan of yz-plane (https://youtu.be/uvPulo7Vfbs)

Figure 6. Scout scan of large field of view (LFoV: 15mm × 15mm × 4.5mm)

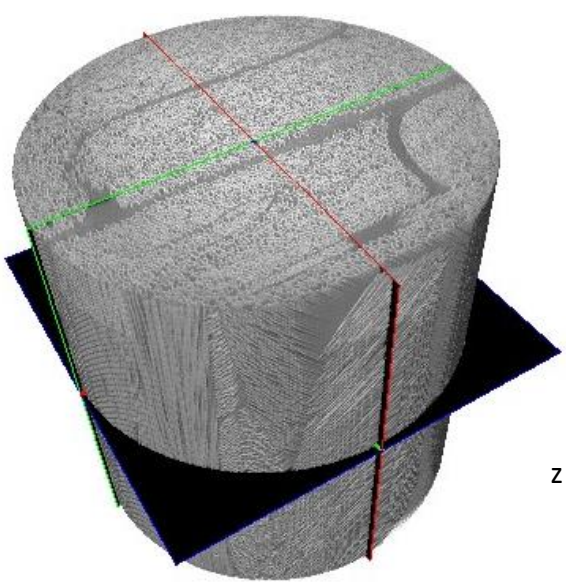

(a) Small scale of view scan region with and indication of the presented slices

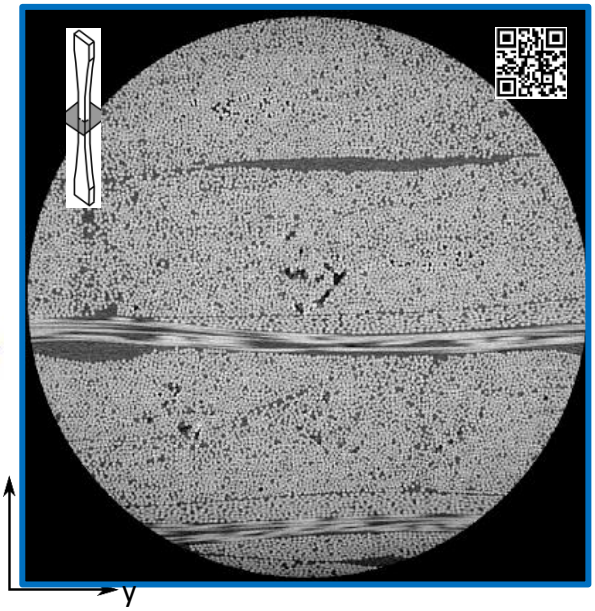

(b) SFoV scan in yz-plane (https://youtu.be/6N5oIVoi1X4)

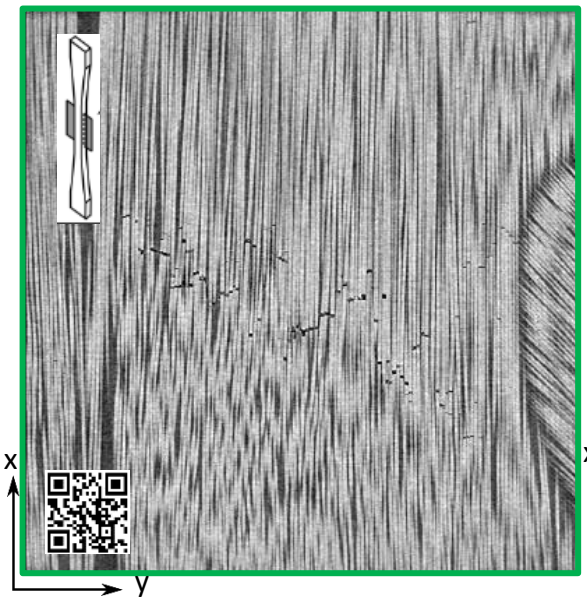

(c) SFoV scan in xy-plane (https://youtu.be/48VZmUs1C-8)

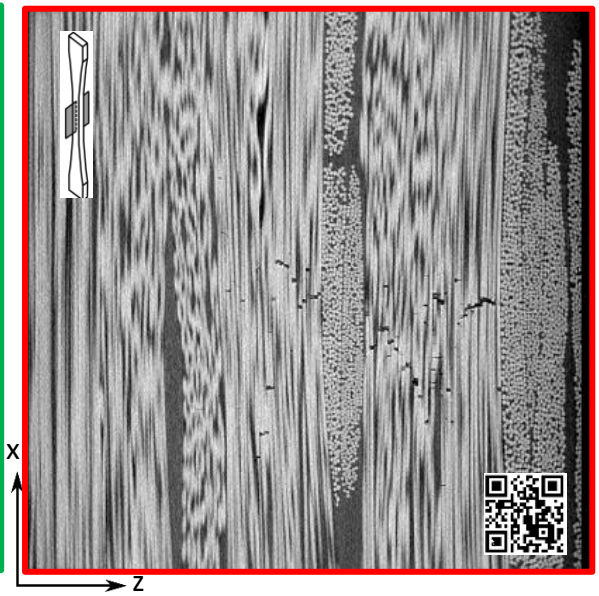

(d) SFoV scan in xz-plane (https://youtu.be/ICjs1Zeg6pU)

Figure 7. Small field of view scan (SFoV: 2.5mm × 2.5mm × 2.5mm)

In figure 7, the results from the zoomed scan is shown. Also here, the selected slice are linked to a QR-code and a URL-link showing a video slicing through the 3D tiff-stack. In figure 7, the voxel-size is 2.5 µm and with an average fibre diameter of D_0=17 µm, it is possible to see the individual fibres. Inside the field of view, a damage region with a lot of fibre failure can be seen. Similar to the scout scan, also for the zoomed scan, the fibre failure is easier to locate in the video than in on selected slice. It can

be observed that the fibre failure region, is following the orientation of the backing bundle just beneath the slice shown figure 7c, something indicating that the fibre failure in the load carrying fibre bundles are controlled or strongly influenced by the present of the secondary oriented backing bundles. From the corresponding video of the region around the slice shown in figure 7c, it can be seen that there in addition to the 45° bundles also is a 90° bundle present at the location close to all the fibre failures indicating that a cross over point not only between the backing and the UD bundle but with multiple cross over points is critical fatigue damage initiation regions.

In the investigated case, the fatigue test has been stopped rather close to the final failure of the sample and the fatigue damage region is rather well developed. Therefore, a further evolution of the fatigue damage is difficult to obtain without running into the final failure of the material. In [4], [11], the same material system has been studied where the fatigue test has been interrupted much earlier in the fatigue life. Thereby, it has been possible using the non-destructive nature of the x-ray techniques obtaining four subsequently 3D x-ray based reconstructed dataset of the same region in the material. From that data-set, it was possible to see how the fibre failure was evolving from a region close to the crossing point of the secondary oriented backing bundles into the load-carrying bundles later during the fatigue loading. In addition, subtracting two aligned 3D reconstructed images obtained with 20.000 fatigue load cycles in between, it was possible to get a 3D reconstruction of the fatigue damage region by simply looking at the difference between the two 3D reconstructions. The 3D reconstructed fatigue damage region can be seen in figure 8.

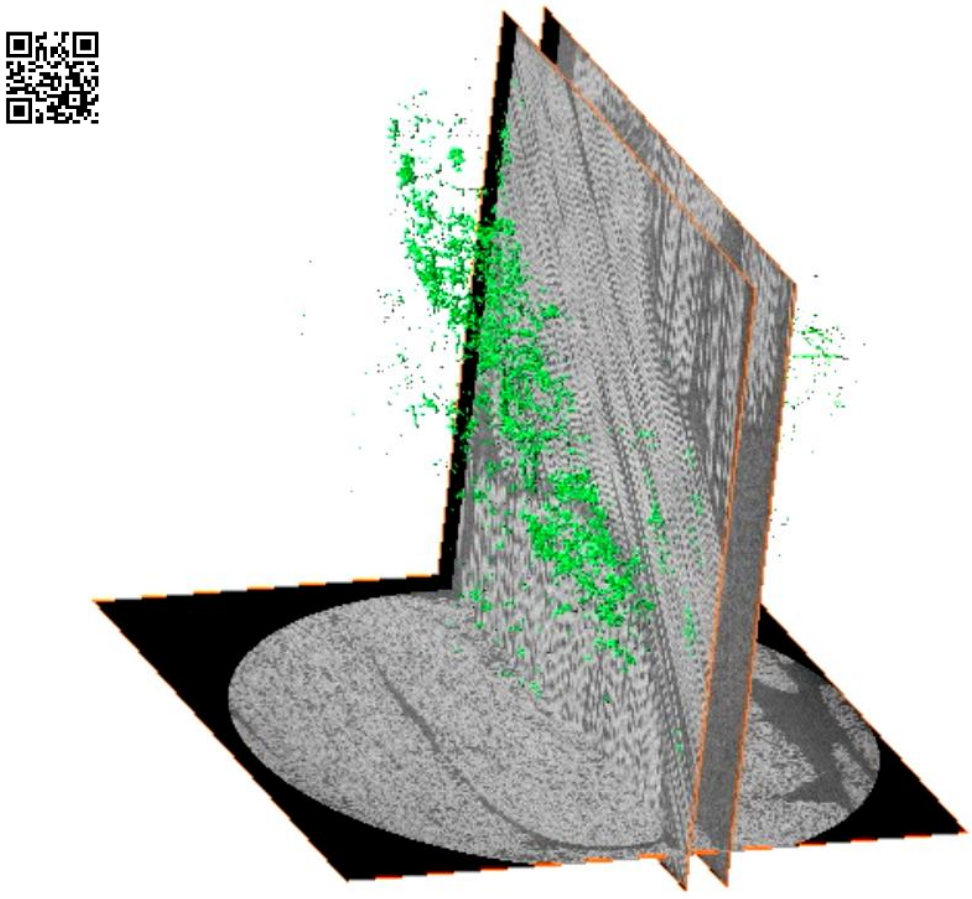

Figure 8. The 3D reconstructed fatigue damage region (https://youtu.be/8tg4aa7Gvks)

5. Conclusion

For the investigated material, it has been found that the tension/tension fatigue damage region is located close to a crossing region of the backing bundles. This region has been located first by investigating a 15mm full cross section area of the test sample. From that scout scan, a fatigue damage region was located. From the small field of view scan, details about the fatigue damage region is obtained such as the orientation of the fiber failure are following the orientation of the backing bundles. This observation for the specific material system has been validated in a number of other similar material system as shown in [3]–[5].

Acknowledgment

Financial support from CINEMA: "the allianCe for ImagiNg of Energy Materials", DSF-grant no. 1305-00032B under "The Danish Council for Strategic Research" is gratefully acknowledged. This research was conducted using x-ray tomograhpy and mechanical testing equipment from DTU Center for Advanced Structural and Material Testing (CASMaT), Grant No. VKR023193 from Villum Fonden.

References

[1] L. P. Mikkelsen, "A simplified model predicting the weight of the load carrying beam in a wind turbine blade," *IOP Conf. Ser. Mater. Sci. Eng.*, vol. 139, pp. 1–8, 2016.

[2] R. P. L. Nijssen and P. Brøndsted, "Fatigue as a design driver for composite wind turbine materials," in *Advances in Wind Turbine Blade Design and Materials*, 2013, pp. 175–209.

[3] K. M. Jespersen, J. Zangenberg, T. Lowe, P. J. Withers, and L. P. Mikkelsen, "Fatigue damage assessment of uni-directional non-crimp fabric reinforced polyester composite using X-ray computed tomography," *Compos. Sci. Technol.*, vol. 136, pp. 94–103, 2016.

[4] K. M. Jespersen and L. P. Mikkelsen, "Three dimensional fatigue damage evolution in non-crimp glass fibre fabric based composites used for wind turbine blades," *Compos. Sci. Technol.*, vol. 153, pp. 261–272, 2017.

[5] K. M. Jespersen, J. A. Glud, J. Zangenberg, A. Hosoi, H. Kawada, and L. P. Mikkelsen, "Uncovering the fatigue damage initiation and progression in uni-directional non-crimp fabric reinforced polyester composite," *Compos. Part A Appl. Sci. Manuf.*, vol. 109, pp. 481–497, 2018.

[6] J. Zangenberg, P. Brøndsted, and J. W. Gillespie, "Fatigue damage propagation in unidirectional glass fibre reinforced composites made of a non-crimp fabric," *J. Compos. Mater.*, vol. 48, pp. 2711–2727, 2013.

[7] K. L. Reifsnider and R. Jamison, "Fracture of fatigue-loaded composite laminates," *Int. J. Fatigue*, vol. 4, no. 4, pp. 187–197, Oct. 1982.

[8] S. Korkiakoski, P. Brøndsted, E. Sarlin, and O. Saarela, "Influence of specimen type and reinforcement on measured tension–tension fatigue life of unidirectional GFRP laminates," *Int. J. Fatigue*, vol. 85, pp. 114–129, 2016.

[9] J. Z. Hansen and R. Østergaard, *The effects of fibre architecture on fatigue life-time of composite materials*. DTU Wind Energy, 2013.

[10] L. P. Mikkelsen, "Observations of microscale tensile fatigue damage mechanisms of composite materials for wind turbine blades [Data-set]." https://doi.org/10.5281/zenodo.1300017, 2018.

[11] K. M. Jespersen and L. P. Mikkelsen, "Ex-situ X-ray computed tomography data for a non-crimp fabric based glass fibre composite under fatigue loading," *Data Br.*, vol. 15, pp. 1003–1005, 2017.